Methods 94 (2016) 120–128

Contents lists available at ScienceDirect

Methods

journal homepage: www.elsevier.com/locate/ymeth

Measuring the micromechanical properties of embryonic tissues

Nicolas R. Chevalier [a,*], Elodie Gazguez [b,c,d,1], Sylvie Dufour [b,c,d,1], Vincent Fleury [a]

[a] Laboratoire Matière et Systèmes Complexes, Université Paris Diderot/CNRS UMR 7057, 10 rue Alice Domon et Léonie Duquet, 75013 Paris, France
[b] UMR144, CNRS-Institut Curie, Paris, France
[c] Université Pierre et Marie Curie, UPMC, Paris, France
[d] Université Paris-Est, UPEC, Faculté de Médecine, Créteil, France

ARTICLE INFO

Article history:
Received 30 April 2015
Received in revised form 21 July 2015
Accepted 4 August 2015
Available online 5 August 2015

Keywords:
Young modulus
Stiffness
Atomic force microscopy
Embryo
Mechanics
Cantilever

ABSTRACT

Local mechanical properties play an important role in directing embryogenesis, both at the cell (differentiation, migration) and tissue level (force transmission, organ formation, morphogenesis). Measuring them is a challenge as embryonic tissues are small (μm to mm) and soft (0.1–10 kPa). We describe here how glass fiber cantilevers can be fabricated, calibrated and used to apply small forces (0.1–10 μN), measure contractile activity and assess the bulk tensile elasticity of embryonic tissue. We outline how pressure (hydrostatic or osmotic) can be applied to embryonic tissue to quantify stiffness anisotropy. These techniques can be assembled at low cost and with a minimal amount of equipment. We then present a protocol to prepare tissue sections for local elasticity and adhesion measurements using the atomic force microscope (AFM). We compare AFM nanoindentation maps of native and formaldehyde fixed embryonic tissue sections and discuss how the local elastic modulus obtained by AFM compares to that obtained with other bulk measurement methods. We illustrate all of the techniques presented on the specific example of the chick embryonic digestive tract, emphasizing technical issues and common pitfalls. The main purpose of this report is to make these micromechanical measurement techniques accessible to a wide community of biologists and biophysicists.

1. Introduction

It is becoming increasingly clear that the mechanical properties of biological tissues at all length scales, from cells to complete organisms, play an important role in determining key developmental events such as differentiation [1], migration [2], and organ [3–5] or body [6–8] formation. It is therefore important to have at hand methods that allow for a precise and quantitative determination of the mechanical properties (stiffness, viscosity, adhesion) of embryonic tissues. Measurements of these properties allow addressing a range of important biological issues, as we now illustrate by a few examples.

- Engler et al. [1,9] demonstrated that mesenchymal stem cells differentiate preferentially to neurons, muscle or bone tissue depending on the stiffness of the substrate on which they are cultured. Durotaxis [10,11], the phenomenon by which cells tend to migrate toward stiffer areas in 2D cultures, has revealed a fundamental mechanism of cell locomotion in mechanically heterogeneous environments. Extending these findings in vivo will require assessing the mechanical microenvironment of cells in their native environment, the tissue.
- Several diseases including fibrosis [12–14], collagen diseases [15] (e.g. brittle bone disease) or cancer [16] are associated to pathological modifications of normal tissue stiffness [17,18], and linked to the abnormal expression or functioning of extracellular matrix proteins involved in tissue mechanical integrity (e.g., collagen, elastin). Animal models are commonly used to better understand the molecular and cellular basis of these diseases. Characterization of the mechanical properties of these knockout or mutant embryonic tissues will better our understanding of the link between genetic mutation and the resulting pathological phenotype.
- Recent research has unveiled the importance of mechanics in the morphogenesis of organs and body structures. For example, neurulation in the early chick embryo [6], mesoderm specification in the drosophila [8], brain fold formation [19], have all been found to result from the mechanical buckling of tissues sheets. The formation of gut loops [4] has been explained as a mechanical coiling instability induced by internal stresses in a conjunctive tissue, the mesentery. Stiffening of organs and embryonic structures is an essential feature of the

* Corresponding author.
E-mail address: nicolas.chevalier@univ-paris-diderot.fr (N.R. Chevalier).
[1] Present address: INSERM U955, Equipe 6, F-94000 Créteil, France.

http://dx.doi.org/10.1016/j.ymeth.2015.08.001
1046-2023/

morphogenesis of an embryo [20]. All of these investigations have relied on measuring the heterogeneous mechanical properties of tissues or tissue assemblies. The importance of mechanical forces and tissue deformability has long been recognized in the area of plant development [21] and is coming nowadays back to the forefront [22] with the advent of sophisticated characterization methods such as the atomic force microscope (AFM).

- The application of controlled mechanical stresses resembling those experienced in vivo during normal embryonic development is a powerful method to understand the link between mechanics and morphogenesis and improve protocols for ex vivo tissue and organ culture. It is well-known that culturing muscle strips requires applying a periodic longitudinal stress to the organ [23]. We are only starting to unveil the importance of mechanical stresses in the formation of other structures such as the lung [24], the heart [25] etc. Furthermore, the determination of the inotropic (contractile) effects on tissues (e.g. heart cardiomyocytes, gut smooth muscle) of signaling molecules and peptides such as Ca^{2+}, neurotransmitter agonists and antagonists is important for understanding their role in embryonic development and for regenerative medicine [26].

The main challenges faced by scientists seeking to determine the mechanical properties of embryonic tissues are the small (μm to mm), soft (in the 10^2–10^4 Pa range) and visco-elastic (giving rise to time-dependent phenomena) nature of the material. In this paper, we present three different methods. The first two methods – uniaxial tensile testing and inflation – are based on applying tensile stress or pressure using elongated glass fibers or pipettes. They can be assembled at low cost and, although we focus on a particular organ – the embryonic gut –, they can be adapted to a wide variety of different tissue types and geometries. The principle of these methods have been elaborated by others [27,28]. Cantilevers in particular have been applied to a wide range of different biophysical problems like the elastic properties of the arterial wall [29], sarcomere contractility [30], embryonic epithelia [31] and cell monolayers [32]. The goal of this paper is to explain in simple terms how they work and to share our experience of some particular methodological issues: fiber fabrication, calibration, attachment to the embryonic tissue, strain and stress extraction using simple ImageJ plugins. In particular, we present an original and versatile tissue attachment technique using a hook formed at the end of the cantilever fiber. The goal of this report is to make these methods accessible to a wider community of biologists and biophysicists. The last part of this report is devoted to the use of the atomic force microscope to determine the elastic properties of embryonic tissue sections. We present a comprehensive AFM sample preparation protocol and nanoindentation maps on whole embryonic tissue sections. To our knowledge, the AFM maps we present are the first (1°) elasticity maps of native unfixed embryonic tissue, (2°) comparisons of AFM indentation results in formalin fixed and unfixed conditions on whole tissue sections, (3°) comparisons of the elastic modulus deduced by AFM with an independent measurement method, bulk uniaxial tensile testing.

2. Uniaxial tension test

The uniaxial tension test we present can be applied to tissue strips, tubes or more complicated geometries such as blastulas [6]. It is a miniaturized version of the tensile force setups that have been used by physiologists to measure muscle tone and contraction characteristics [33]. Typical forces that must be applied to embryonic organs to measure their linear elastic properties are in the range 0.1–10 μN. It is difficult to find commercially available force gauges suitable for this force range. Moreover, non-invasive attachment of the embryonic organ to the force gauge remains a major technical issue. Here we show how glass fiber cantilevers can be fabricated and used to both measure force and provide anchoring of the sensor to the embryonic tissue. Deformation is measured from particle image velocimetry analysis of movies of the organ as it is put under increasing mechanical tension. The measurement can be performed in a thermalized bath of culture medium or physiological buffer.

2.1. Fiber fabrication and calibration

The angular sensitivity (angular deflection of the fiber per unit force) of a cylindrical fiber of length L, diameter d and material elastic modulus E scales as $s \propto L^2/2Ed^4$. Maximizing the sensitivity of the fiber therefore requires making them as long and thin as possible. We fabricate such fibers by heating glass Pasteur pipettes with a flame and manually pulling on them. With some training, it is possible to fabricate fibers with very high sensitivities (typically up to 10°/μN). After pulling, bends can be added to the design of the fiber. As a general rule, the heavier parts of the pipette will be pulled down by gravity when heated, while the lighter ones (e.g. pipette end) will be drawn up by the convection currents of the flame. Fig. 1a shows a small hook that was formed by quickly applying heat with a Bunsen burner flame to the end of the fiber, causing it to curl. The final form of the hook can then adjusted by cutting with a silicon carbide blade.

After fabrication, the fiber can be calibrated by fastening small weights of known mass at the end of the fiber and measuring the resulting deflection (Fig. 1a). The weights we use are thin pieces of wire. The linear mass λ (g/m) of a long (~1 m) piece of wire is first measured with a balance. For very sensitive fibers, we recommend using ultra-fine metal (e.g. copper) wire; thicker plastic or metal wire can be used for less sensitive fibers. We then cut small pieces of length l_i (if necessary measured using a binocular) resulting in a set of masses $m_i = \lambda l_i$. A hook or a stop (small ball of glue or molten glass) at the end of the fiber prevents the weights from slipping off the fiber during calibration. For very sensitive fibers ($s > 1°/\mu N$), the fiber and weights should be immerged in a liquid to abolish any perturbations from air currents and electrostatic forces. For fiber sensitivities <1°/μN, calibration can be performed in air. Fig. 1b shows a typical calibration curve, we found it to be linear up to at least 30° deflection. Once calibrated, fibers should be stored in a safe environment; they can be used for years if handled carefully.

2.2. Measurement setup

Fig. 1c shows the schematic setup of a uniaxial embryonic tissue tensile test. One should be especially watchful of the following issues:

1. Attachment of the tissue. One end of the tissue can be conveniently immobilized by lining the container bottom with a thin (~1 mm) sheet of 1:50 Polydimethylsiloxane (PDMS, Sylgard silicon oil) so that the tissue can be pinned using ultra-fine (Ø = 50 μm) needles (Euronexia). PDMS is commonly used as a cell-culture substrate and is optically clear, so that the tissue can be illuminated from below. Attachment of the tissue to the cantilever depends on tissue geometry. For tissue strips, or tubes, such as the gut depicted in Fig. 1c–e, we have found that forming a small hook (Fig. 1a) by applying heat at the pipette end allowed for an easy, robust, and minimally invasive way of securing the organ to the fiber. For tissue sheets, at least two points of attachment are required. This can for example be

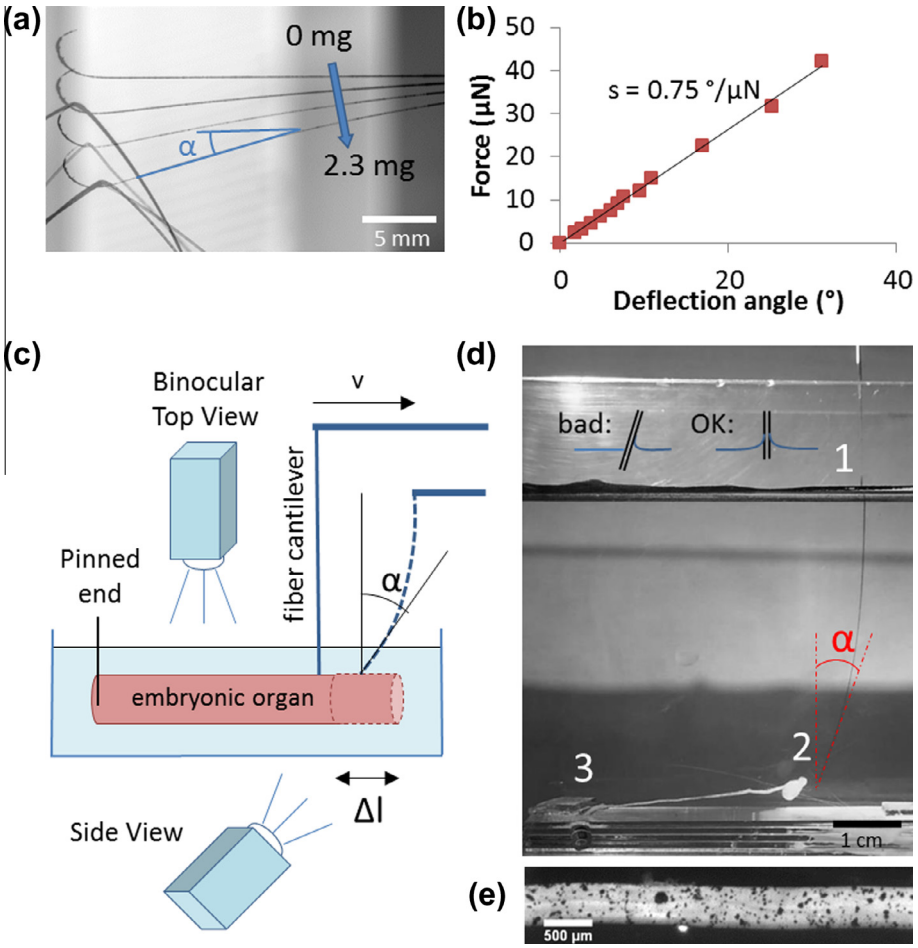

Fig. 1. Fiber cantilever calibration and measurement setup. (a) Four overlaid pictures of the unloaded fiber and after it has been weighted with three increasing weights (wires of increasing length). For each weight, the fiber deflection angle α is measured. The complete fiber is about 10 cm long. (b) The resulting deflection angle vs. applied force calibration curve is linear for small fiber deflection angles (up to 30°); the inverse of the slope gives the sensitivity of the fiber. (c) Scheme of the uniaxial tensile test. The fiber support is pulled at a speed v by a motorized stage. Strain and stress are monitored by the "side view" camera. An additional camera mounted on a binocular can monitor deformation for high resolution strain mapping, Shape of the gut and fiber at rest and after a force α/s, resulting in a deformation Δl is applied, are indicated respectively by full and dotted lines. (d) Side view of a 10-day old embryonic chick gut mounted in the uniaxial traction setup. Medium level in the trough is high so that the fiber always forms a 90° angle with the air–water interface (1), even when loaded. The embryonic stomach (2) provides an anchor in which the hook at the end of the fiber can be inserted. The organ is immobilized at its other end (3) by a glass plate or can be pinned to a Sylgard-lined container. (e) Higher magnification view of an 8-day old embryonic chick midgut sprinkled with carbon particles for Particle Image Velocimetry (PIV) analysis of deformation, as seen with the "top camera".

achieved by gluing a fine rod (e.g., needle or glass fiber) perpendicularly to the cantilever end. The tissue sheet is then drawn over the two extremities of the rod. Other ways of attaching embryonic tissue include using glue (e.g. Vetbond surgical glue), gels (low melting-point agarose) or electrocauterization. Care should however be taken when applying these methods as they might affect the native mechanical properties of the tissue.

2. Capillary forces. When the fiber cantilever enters the physiological medium – air interface at an angle, torque is generated by capillary forces and bends the fiber (scheme Fig. 1d, "bad"). This torque may modify the apparent sensitivity of the fiber. If the capillary force acts close to the fiber tip (very low medium levels), the deflection angle due to capillary forces can be estimated as $\alpha_{cap} = s\gamma d\cos^2\theta$, where s is the pipette sensitivity, γ the surface tension of the medium, d the fiber diameter and θ the angle between the fiber and the vertical. This effect can be minimized by (1°) using high water levels, such that the torque exerted by capillary forces has a small lever arm and acts in a region where the fiber is thicker, (2°) making sure the fiber and interface form a close to 90° angle (scheme Fig. 1d, "OK") when the fiber is at rest. In this configuration, the meniscus is symmetric and no torque is generated. Small deflections of the fiber-medium angle at the level of the medium-air interface (due to loading of the fiber end) will therefore lead to a minimal amount of capillary torque. Surfactants such as soap can be used to check the influence of capillary forces in a given setup: if the fiber angle/position does not significantly change upon adding soap, capillary forces can be deemed negligible.

The other end of the fiber is secured to a stepper motor (Newport M-UTM linear stage with ESP300 controller) that allows pulling on the tissue with a constant speed v. For an organ of length L, the strain rate is then given by v/L. We used typical speeds $v \approx 50\ \mu m/s$ giving strain rates on the order of $0.1\ min^{-1}$, at a 1 Hz image sampling frequency. In general, it is necessary to perform measurements at different strain rates and different samples should be compared at the same strain rate. For embryonic gut, we have found that the elastic modulus does not depend on strain rate as long as the latter is higher than the typical viscoelastic relaxation time of the tissue, meaning that the tissue does not significantly relax over the time it takes to perform the tensile test (~30 s). It is crucial to let the embryonic organ relax (~30 min) and come back to its initial length before and between each tensile test. Under these conditions, we found that elastic modulus variations between successive tensile tests on the same sample were small,

within ±10–20% of the average. If no stepper motor is available, the fiber can be translated with the help of a micromanipulator vise rotated manually or via a motor.

A camera (we use a 1600 × 1200 px Stingray FT-201, Allied Vision Technologies, equipped with a Computar macro lens x0.3–1) looking at the setup sidewise monitors fiber deflection over the course of the tensile test. This camera can also be used to monitor organ deformation, as shown in Fig. 2. The elastic properties of the sample can be determined with a high spatial resolution by monitoring strain by using a separate camera mounted on a binocular or a microscope (Fig. 1c, "top view" and representative image in Fig. 1e). When using a separate camera for strain monitoring, it is important for it to be synchronous with the "stress" camera so that stress and strain state of the organ can be unambiguously determined at each time point.

Deformation of the sample can be automatically extracted from a movie granted the tissue has sufficient texture. When monitoring strain at high magnification, the cells of the tissue might provide this texture when illuminated by diffuse (e.g., 90° illumination) or transmitted light. Reflected light should by all means be avoided, as the shimmering reflections of the tissue surface cannot be used to track displacements. At lower magnifications, texture can be enhanced by adding extraneous particles. We have found ground carbon powder (soot) to be especially convenient for that purpose as the particles are readily dispersed in a physiological buffer, have the required size (∼1–10 μm), adhere well to the embryonic tissue, and provide excellent contrast. A representative movie from which the stress and strain data in Fig. 2 were extracted is provided as Supplementary material (Movie 1).

2.3. Data analysis

The main steps of the data analysis process are summarized in Fig. 2. We note x_{ij} the x coordinate of point number i in frame number j of a movie. For strain analysis, N regularly spaced points of coordinates $(x_{1,1} \ldots x_{N,1})$ in the 1st frame of the movie are selected along the segment of tissue to be analyzed. A Particle Image Velocimetry (PIV) software such as the Tracker plugin ([34], courtesy of O. Cardoso) is used to track the coordinates of these points in the movie. Further data treatment can be handled using a programming environment such as Matlab. The displacement of each point i in frame j relative to the first image in the movie, $\Delta_{ij} = (x_{ij} - x_{i1})$ is first computed. Fig. 2b shows a typical example of the displacement as a function of position along the length of the organ for 6 different frames in a movie. The strain (deformation) in each frame is the slope of the position-displacement curve

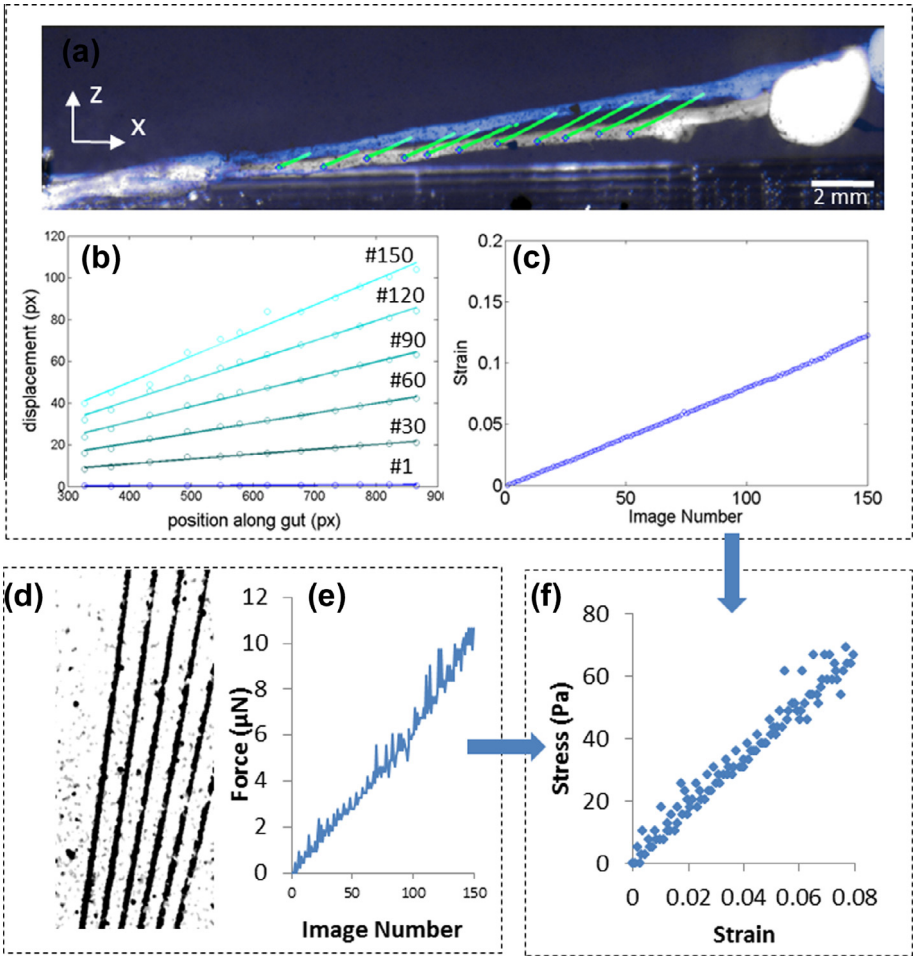

Fig. 2. Strain and stress analysis of a 6.5-day old embryonic midgut. (a) The initial (rest) and final (maximum tension) position of the organ are superimposed in this image, in white and blue respectively. The green lines indicate the trajectories from the rest to the tensed state of points spaced regularly along the length of the organ. The trajectories are automatically computed for the 150 frames of the movie by PIV tracking. As the organ is immobilized at its left end, the displacement increases from left to right. (b) x-component of displacement as a function of the x position along the gut, for the points shown in (a), for frames #1, 30, 60, 90, 120 and 150 in the movie. The slope of each curve is the strain. (c) Strain extracted for all frames in the movie. (d) Overlay of five different fiber positions during tensile test, fiber angle is automatically extracted from the movie by the Hough Linear ([38], courtesy of M. and W. Burge) ImageJ plugin. (e) The resulting force exerted by the fiber can then be computed for all frames in the movie. The stress is the force F divided by the organ cross section A: $\sigma = F/A$. (f) Putting (e) and (c) together, the stress–strain characteristic of the embryonic organ can be plotted, the slope is the elastic modulus.

[35] and can be extracted to yield the strain for all frames in the movie (Fig. 2c). Stress is extracted from a movie of fiber deflection. Fiber angle can be automatically computed by thresholding the movie to extract a line and using the Hough Linear algorithm (Fig. 2d). Since deformations are evaluated relative to the first image in the stack, fiber deflections should also be evaluated relative to the first image, i.e., the force F_j applied in frame j (Fig. 2e) is defined as $F_j = (\alpha_j - \alpha_1)/s$ where s is the fiber sensitivity (°/N), and α_j the fiber angle in frame j. The first image does not need to be the zero-stress state; in certain circumstances, in can be useful to apply a small pre-stress to unfold the tissue. The pre-stress should however be kept small if the linear elastic properties of the sample are to be measured. Noise in the force curve (Fig. 2e) is due to the fact that the line representing the fiber is thick (Fig. 2d), causing variations in the output of the Hough linear algorithm: this can be improved by optimizing lightning conditions of the fiber during the tensile test and edge detection and thresholding during processing of the movie. As can be seen in Fig. 2a, the fiber slightly lifts the organ in the z-direction during the extension. As a result the force exerted by the tissue on the fiber does not have a rigorously constant direction (as when applying the weights during the calibration procedure). In our case this z-lift resulted in minor corrections to the applied stress (<5%) but depending on fiber length, applied stress and tissue type, it may be important to correct for this angular deviation either during the measurement (by changing the z-position of the fiber during the extension) or during data analysis. The force applied to the tissue should finally be converted to a stress by dividing by the local tissue cross section A. For the approximately cylindrical midgut of Fig. 2a and since the gut lumina is small, the section is well approximated by $A = \pi r^2$, where r is the gut radius as measured with a high-magnification binocular. In general, as the diameter can be somewhat variable along the length of the segment analyzed, uncertainties on tissue cross section are one of the main contributions to the uncertainty of the final elastic modulus. Once the strain and stress have been determined for all frames in the movie, they can be combined to yield the stress–strain characteristic of the tissue. For biological tissues, the stress–strain plot is usually linear for small strain values; the slope in this region is the linear elastic modulus of the material. Strain stiffening [36] is often observed at higher strains for biological gels or tissues. In a study to determine the evolution of the elasticity of the embryonic gut at different developmental stages [37], we found that the uncertainty on elastic modulus was ±20–30%. This uncertainty originates from the determination of gut diameter for segments that are not strictly cylindrical (e.g., the hindgut), whereas it is smaller and dominated by stretch-to-stretch variability for the more straight cylindrical segments (e.g., the jejunum). We found sample-to-sample variability at a given developmental stage to be in the range 10–20%.

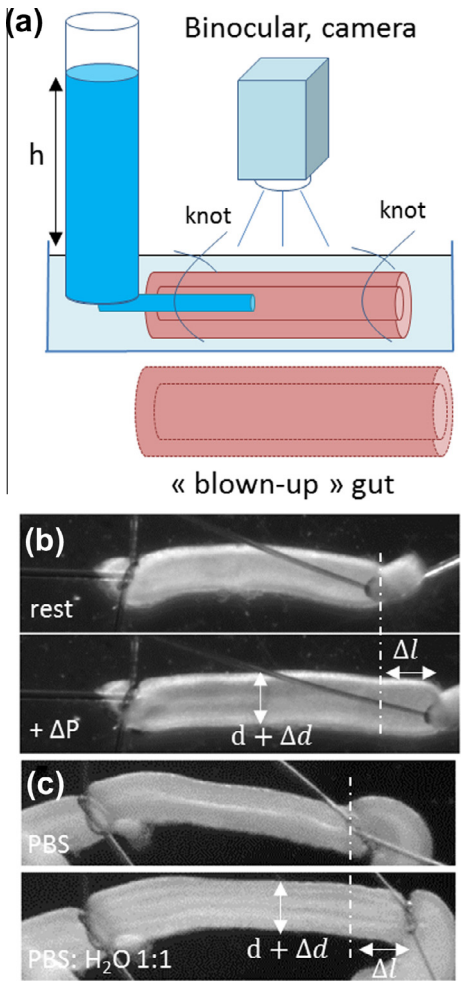

Fig. 3. Applying pressure. (a) Scheme of setup. A cannula (pulled glass pipette) is inserted in the lumina. The cannula gut junction and the gut are sealed by tying a knot with a thin hair. A column of physiological buffer of height h applies a pressure $\Delta P = \rho g h$. (b) Example of resting (top) and pressurized (bottom) state using the setup described in (a), 8 day old gut. The cannula is seen on the left side. Gut length increases a factor 1.5–2 more than gut radius. (c) An osmotic shock also triggers a pressure increase, in a 7.5-day-old gut. Top: physiological PBS buffer. Bottom: PBS: H_2O 1:1 mixture. As the lumina is only accessible through small openings at the rostral (oesophagus) and caudal (cloaca) end, replacement of the fluid in the lumina by diffusion through these openings is slow and the liquid in the lumina can therefore be assumed to have the tonicity of PBS and/or luminal fluid. Note that the knots shown in this experiment are used here as fiducial markers and are not required for the generation of osmotic pressure in the gut tissue, as segments lying outside of these knots also swelled. As when applying pressure via a cannula, we found that the gut length increased a factor 1.5–2 more than gut radius after placing the organ in PBS:H_2O 1:1.

3. Quantifying stiffness anisotropy

We have so far only considered tissue elasticity along one direction. Owing to the specific orientation of cells and extracellular matrix, many tissues present anisotropic stiffness properties. In the gut for example, the stiffness along a direction parallel to the gut axis is different from the orthoradial (i.e., along the gut perimeter) stiffness. To probe the orthoradial stiffness, it is necessary to apply a stress perpendicularly to the gut wall. This can be achieved by applying pressure to the lumina of the organ via a cannula, as depicted in Fig. 3a. Granted that the cannula-organ junction and the free end of the organ are both sealed tight, the pressure inside the lumina can be controlled by regulating the height h of a water column, $\Delta P = \rho g h$. For embryonic tissues ($E \sim 1000$ Pa), a few centimeters of water are usually sufficient to induce significant deformations. We have found that thin hair strands (Fig. 3b) or fine suture thread can be used to tie micron-size knots to seal a segment of gut. We caution that it is in general difficult to ensure complete tightness of the embryonic organ and cannula in this setup. If the longitudinal modulus of an organ has already been determined by the method described in Figs. 1 and 2, it is however possible to determine the orthoradial modulus of an organ by comparing the relative distensions along the longitudinal and radial directions induced by a pressure increase in the lumina, even when the organ is not perfectly sealed tight. This is shown in Fig. 3b, where a pressure increase applied through a column of physiological medium triggers an elongation Δl of the gut length and an increase in diameter Δd. For a pressurized cylindrical vessel of outer radius R, it can be shown [39] that the orthoradial wall tension at the gut outer border $\sigma_\theta(R)$ is two times higher than the wall tension at the

hemispherical end σ_z, i.e., $\sigma_\theta(R) = 2\sigma_z$. Defining the orthoradial and elastic moduli E_θ and E_z, respectively as $E_\theta = \sigma_\theta(R)/(\frac{\Delta d}{d})$ and , $E_z = \sigma_z/(\frac{\Delta l}{l})$ the ratio of orthoradial to longitudinal elastic modulus can be deduced from the ratios of deformation: $E_\theta/E_z = 2(\Delta l/l)/(\Delta d/d)$. In Fig. 3b, we experimentally find the elongation $\Delta l/l$ to be a factor 1.5–2 higher than the diameter change $\Delta d/d$, which means that the orthoradial elastic modulus E_θ is a factor 3–4 higher than the longitudinal elastic modulus E_z. This confirms the strong stiffness anisotropy in tubular organs such as the gut. Stretching and inflating are complementary methods as they can be applied successively to yield quantitative values of both E_z and E_θ on the same sample. We finally note that a simpler way of increasing the internal pressure of a tissue is to apply an osmotic shock by placing it in a hypotonic solution. In Fig. 3c a photograph of an embryonic gut is shown in a physiological PBS buffer and after it was placed in a hypotonic PBS:H_2O 1:1 mixture. The gut elongates and increases in diameter. We find the osmotic shock to yield a similar ratio 1.5–2 of elongation over diameter increase than that found by applying hydrostatic pressure to the gut lumina. Changes in osmotic pressure have been previously used to apply pressure to tumor spheroids [40] and also for the mechanical characterization of articular cartilage in free-swelling tests [41]. Osmotic swelling properties may vary according to tissue type [42]. For example, in the case of the gut, the amount and kinetics of swelling of the epithelium most probably differ from those of cells located, say, in the muscularis. Nonetheless, the pressure pattern remains radially symmetric and these differences should not reflect on the ratio E_θ/E_z. In general, we believe that this osmotic pressure approach can easily give access to tissue relative elastic modulus contrasts along different directions when the cells in the sample are sufficiently homogeneous (e.g. isolated epithelium) or symmetric (as in the case of the GI tract).

4. Atomic force microscopy

Biological tissues are composed of different layers. A section of gut for example is organized in concentric sheets, the mucosa (epithelium), submucosa (connective tissue), muscularis (muscle layer) and serosa (outermost layer). The uniaxial tensile test we presented measures the average modulus of these different tissue types. In many instances, it may be desirable to measure the elastic properties of a particular tissue layer. In adult artery biomechanics, this is achieved by isolating each tissue layer and measuring their elastic properties separately. As dissociation of embryonic tissues is generally difficult, an alternative method consists in reducing the size of the probe and measure the mechanical properties of embryonic tissue cross sections. This can be achieved by nano-indenting the tissue using an atomic force microscope. Atomic force microscopy has been used extensively to measure stiffness of substrates for cell culture [43] and the stiffness properties of individual cells [44]. Studies pertaining to whole native tissues are however more rare: they concern mainly bones [45], cartilages [46] or arteries [47,48] and usually feature only topographical data; elastic modulus properties have only been studied in a few cases [47,49]. The topography of live embryonic tissue has recently been studied with the AFM [50]. One recent study has used the AFM to measure mechanical properties of blastulas at gastrulation stage [51], but to the best of our knowledge we present here the first elastography maps of live embryonic tissue.

4.1. Sample preparation

One of the key issues in AFM imaging and nano-indentation is to properly and non-invasively hold the sample in order for it not to be dragged along by the cantilever tip during scanning. Agarose gel has been used to embed plant samples and embryonic tissues for AFM studies [22,50]. Other sample holding techniques have been reported [48]. We have used agarose gel and found it appropriate to (1°) keep the tissue in a hydrated state, (2°) mechanically immobilize it, (3°) provide support to perform tissue sections with a surface smooth enough for the AFM, (4°) fix the tissue with formaldehyde after the AFM scan and perform immunohistochemistry. We use low-melting point agarose (Type VIIA, Sigma) solutions in PBS at 3% w/w. After boiling, we cool the agarose solution down back to 37 °C by placing it in a heated water bath. Any evaporation losses should be corrected by adding distilled water to guarantee iso-osmotic conditions. At this point the agarose is poured in a small Petri dish (Ø = 40 mm) and the embryonic organ is transferred with a minimal amount of physiological buffer to the liquid agarose. The agarose is then further cooled to 20 °C, the embryonic tissue is kept positioned in the bulk of the gel with the help of tweezers. It is important not to perturb the gel in the few tens of seconds before it gels, as this can significantly reduce gel mechanical integrity and compromise proper sample holding. Complete solidification of the gel takes about ~30 min and can be monitored by measuring the light diffused by the gel in a time-lapse movie. After the gel solidifies, sections can be performed using either a vibratome, or a double-bladed cutter. We found it convenient to fabricate our own double-bladed knife by gluing two razor blades (Gillette) to a spacer. The thickness of the spacer and of the blades (typically ~100 μm each) defines the total thickness of the slices. Section thickness should be a factor ~10–100 higher than the maximum AFM indentation depth (typically a few μm) to ensure that only the elasticity of the tissue is probed and not that of the underlying substrate. We used 1 mm thick slices. It is important that the two section planes be parallel so that the section is as horizontal as possible for AFM scanning. The slices can then be glued to Petri dish bottoms using liquid low-melting point agarose as a glue. Vetbond glue can also be used but may lead to difficulties in viewing the sample in transmitted light as it becomes white when reticulated. Using thick samples is useful to help making sure that no Vetbond or agarose comes into contact with the surface to be analyzed. The sample should be submerged in PBS just after gluing to the Petri dish bottom. It can now be transferred to the AFM stage and the AFM tip can be submerged. It is again appropriate to check with a time-lapse movie at high magnification that a stationary state is reached where the tissue sample remains immobile over the time it takes to perform a scan (typically 1–30 min depending on resolution), as slight temperature variations may cause the gel to swell or contract and the tissue sample to be displaced.

4.2. Scanning

As embryonic tissues are notoriously soft [52], very low bending stiffness cantilevers must be used to maximize signal to noise ratio. We used $k_{measured} \sim 60$ mN/m ($k_{announced} = 30$ nN/m) rectangular silicon cantilevers (Novascan) functionalized with a 10 μm borosilicate glass beads. A 1 nN maximal indentation force yielded typical indentation depths of 0.5–3 μm for live embryonic tissue and about 0.1–0.5 μm for formaldehyde fixed tissue. These values are appropriate as they are below the radius of the indenter (5 μm). We typically use indentations speeds of up to 50 μm/s. Resulting strain rates for each indentation are on the order of 10^3 min^{-1}, much higher than those used for the tensile test. As the apparent elastic modulus of cells [53] can vary with indentation speed, is it important when comparing different samples to keep a constant indentation speed. The AFM we use is a JPK Nanowizard I equipped

with the CellHesion platform, which allows for a 100 μm-displacement amplitude of the tip along the *z*-axis during a scan. We found this latter feature to be essential as it made it possible to scan large areas (100 × 100 μm) without exiting the *z*-scan range. The total number of indentations in a scan, *z*-travel length and indentation speed along the *z*-axis determine the total duration of a scan. As we found unfixed tissue samples to present altered mechanical properties ~6 h after dissection, it is important to choose a combination of these parameters that allows to retrieve the required information in a timely manner.

4.3. Analysis

In Fig. 4a, we show one example of a tissue section overlaid with 3 elasticity maps obtained by AFM indentation. Elasticity was deduced by fitting the force-indentation depth curves using the Hertz model. The concentric ring organization of the different gut layers can readily be distinguished in the elasticity maps. We found the epithelium (innermost region) to be the stiffest region, followed by the muscularis (outermost region) while the submucosa, which is located between the epithelium and muscularis is softest. AFM elastic moduli increased with developmental stage from E4 to E8 [37]. Similar developmental stiffening was observed for chick embryonic hearts [20]. The AFM elastic moduli we find are in the range 10–200 Pa, in line with AFM measurements performed on chicken embryo blastula explants at gastrulation stage [51]. It is also comparable to the elastic modulus of cultured leukocytes [54] or neurons [55], but much softer than many other cell types [56] like fibroblasts (0.6–12 kPa) or endothelial cells (0.2–18 kPa). Comparisons between AFM results obtained on 2D cultured cells with our tissue-scale measurement are not straightforward. The embryonic tissue we consider is composed of cells and extra-cellular matrix (ECM) and the cells in the not yet fully differentiated mesenchyme of the gut are not densely packed. After performing live tissue sections, we therefore probe the properties of cells and of the surrounding ECM. Moreover, as the cantilever bead is lowered on the tissue, cells can be displaced, rather than being compressed. This situation is different from most AFM studies performed on 2D cultured adherent cells [56], where there is less or no ECM, where cantilever tip radii are usually much lower (typically ~100 nm) and where adherence of the cell to the substrate bottom reduces the overall displacement of the cell during indentation. The fact that we find higher elastic moduli in the epithelium than in the mesenchyme lends support to this explanation: the cells in the epithelium are more difficult to displace as they are bound together by tight junctions and anchored to the basal lamina. Finally, performing the transverse section also disrupts the surface mechanical properties of the gut by damaging cells and sectioning of fibers and cell–cell connections. To assess the amount of cell death, we used Trypan blue staining. This dye is rapidly excluded by living cells but stays inside the cytoplasm of dead cells, coloring them blue. We detected the presence of stained (dead) cells at the sample surface (Fig. 4d). Epithelial cells were never stained and staining was also reduced in the region of the muscularis. In spite of this unavoidable damage (the organ has to be dissected and sliced open to perform AFM inside the tissue), the protocol we describe gives access to non-trivial information concerning the relative elastic modulus variations at different developmental stages [37], and for different histological regions within one tissue section (Fig. 4).

The elastic modulus values deduced from AFM indentation are also almost an order of magnitude lower than the values deduced from uniaxial tensile testing, (typically AFM: ~20–200 Pa, tensile testing: ~200–1000 Pa). In addition to the surface damage discussed above, we believe another possible explanation of this discrepancy could be due to the fact that the tensile test measures the

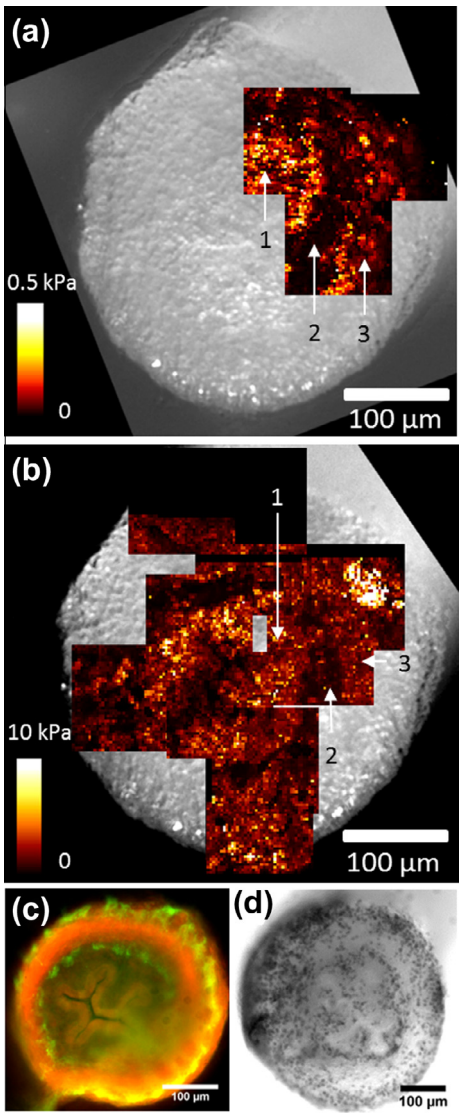

Fig. 4. Atomic force microscopy maps of an 8-day old embryonic midgut, embedded in a 3% agarose gel. (a) Three elastic modulus maps obtained within 3 h after dissection, overlaid on a microscopy image. Dark/light pixels correspond to soft/hard regions respectively. The concentric organization of the gut layers is apparent in the modulus maps: the mucosa (1, it comprises the epithelium) and muscularis (3) are stiff and separated by a softer region, the submucosa (2). Elastic modulus values are very low: 0–0.5 kPa. Acquisition parameters are: 1nN indentation force, 50 μm/s indentation speed, 10 μm indentation bead diameter, scan size 100 × 100 μm, 40 × 40 pixels. (b) Elastic modulus maps of the same section after it was fixed with formaldehyde (room temperature, 2 h). The elasticity contrasts of the three concentric regions are preserved, but the absolute elastic modulus range is a factor 20 higher: 0–10 kPa. Acquisition parameters are the same as in (a). (c) Fixed agarose sections can be immuno-labeled for smooth muscle (red, anti-α smooth muscle actin antibody, Abcam ab5694) and enteric neurons (green, TUJ1 antibody, Abcam ab14545) and the resulting images put in registry with AFM elastic modulus or adhesion maps. The peripheral ring of neurons and smooth muscle are part of the muscularis; the inner ring of neurons is in the submucosa; epithelium surrounding the lumina can also be readily distinguished. (d) Representative Trypan blue (Life Technologies) staining of freshly cut sections of E9 gut.

section-averaged tensile modulus while the AFM measures the local compressive modulus: longitudinal fibrous structures (e.g. collagen, elastin) which are in a tensile state in the traction assay likely contribute less to the elasticity of the organ than when under compression (AFM).

To obtain the mean elastic modulus of a particular region, it is possible to average over particular regions of each stiffness map. For example the mean elastic modulus of the mucosa (white arrow

1 in Fig. 4a) of the freshly dissected tissue is 112 ± 82 Pa, where the uncertainty is the mean roughness, which gives a good description of elastic modulus variations of the surface. For the submucosa (white arrow 2 in Fig. 4a), we find 22 ± 9 Pa. Fig. 4b shows 12 elastic moduli maps of the same tissue section after it was formaldehyde fixed for 2 h. The same general contrasts of elasticity between epithelium (mucosa), muscularis and submucosa are found after fixation, but average elastic moduli were found to be a factor ~25 higher after fixation. A similar stiffening (factor 40) was measured on single cells after treatment with glutaraldehyde [57]. Fig. 4c finally shows that thick agarose gel tissue sections can be treated by immunohistochemistry (IHC) either before or after nano-indentation to reveal the important cell types and histological layers within the sample. An important potential of the technique we present is therefore its ability to make cross-correlations between AFM elasticity maps and histological data. In agreement with other investigators [50], we found that AFM scanning was easier after formaldehyde fixation, as the higher elastic modulus resulted in smoother indentation curves and the tissue remains stable over the course of the measurement. Our measurements show that the same qualitative elasticity contrasts between muscularis, mucosa and submucosa are conserved before and after fixation of the tissue with PFA. We note that the AFM can also be used to retrieve local adhesion (force required to detach the indenter bead upon retraction from a particular tissue region) maps and cross-correlate them with histological data.

5. Conclusion

We have presented how μN forces can be applied using a fiber cantilever or a pressurization cannula, and how the resulting deformation can be read out to extract the elastic properties of embryonic tissue. The atomic force microscope (AFM) can be used to extract elasticity and adhesion maps of embryonic tissue sections at a μm scale. We have described an AFM sample preparation protocol, assessed the effects of formaldehyde fixation on elasticity maps and compared the Young moduli obtained by AFM with those obtained from other bulk measurement techniques.

These micromechanical techniques make it possible to determine the evolution of tissue elastic properties over the course of embryonic development, measure viscoelastic properties of tissue [58], determine quantitatively mechanical disruptions in normal and pathological conditions, investigate correlations between cell mechanical environment and cell migration and differentiation behavior, determine the contributions of specific molecules to elasticity by selectively removing them using enzymes (e.g. collagenase or elastase [59]), assess the contractile force (inotropic effect) generated by molecules on embryonic organs and finally apply controlled forces over long time periods to tissues and organs in culture to evaluate their impact on biological processes.

6. Ethics

Experiments were performed in accordance with the ethical guidelines of the INSERM and CNRS. The authors declare no conflict of interest.

Acknowledgments

This work was funded by ANR-12-BSV2-0019 ENSINTED and by the Labex “Who Am I?”. NRC was supported by a Labex “Who Am I?” postdoctoral fellowship. E.G. was supported by a PhD fellowship from the Ministère de l’Enseignement et de la Recherche.

Appendix A. Supplementary data

Supplementary data associated with this article can be found, in the online version, at http://dx.doi.org/10.1016/j.ymeth.2015.08.001.

References

[1] A.J. Engler, S. Sen, H.L. Sweeney, D.E. Discher, Cell 126 (2006) 677.
[2] J.R. Lange, B. Fabry, Exp. Cell Res. 319 (2013) 2418.
[3] A.E. Shyer, T. Tallinen, N.L. Nerurkar, Z. Wei, E.S. Gil, D.L. Kaplan, C.J. Tabin, L. Mahadevan, Science 342 (2013) 212.
[4] T. Savin, N.A. Kurpios, A.E. Shyer, P. Florescu, H. Liang, L. Mahadevan, C.J. Tabin, Nature 476 (2011) 57.
[5] N. Desprat, W. Supatto, P.A. Pouille, E. Beaurepaire, E. Farge, Dev. Cell 15 (2008) 470.
[6] V. Fleury, N.R. Chevalier, F. Furfaro, J.L. Duband, Eur. Phys. J. E (2015).
[7] E. Farge, Curr. Top. Dev. Biol. 95 (2011) 243.
[8] T. Brunet, A. Bouclet, P. Ahmadi, D. Mitrossilis, B. Driquez, A.-C. Brunet, L. Henry, F. Serman, G. Béalle, C. Ménager, F. Dumas-Bouchiat, D. Givord, C. Yanicostas, D. Le-Roy, N.M. Dempsey, A. Plessis, E. Farge, Nat. Commun. 4 (2013) 2821.
[9] J.R. Tse, A.J. Engler, PLoS One 6 (2011) e15978.
[10] C.-M. Lo, H.-B. Wang, M. Dembo, Y. Wang, Biophys. J. 79 (2000) 144.
[11] L.G. Vincent, Y.S. Choi, B. Alonso-Latorre, J.C. del Alamo, A.J. Engler, Biotechnol. J. 8 (2013) 472.
[12] P.C. Georges, J.-J. Hui, Z. Gombos, M.E. McCormick, A.Y. Wang, M. Uemura, R. Mick, P.A. Janmey, E.E. Furth, R.G. Wells, Am. J. Physiol. Gastrointest. Liver Physiol. 293 (2007) G1147.
[13] R.L. Lieber, S.R. Ward, Am. J. Physiol. Cell Physiol. 305 (2013) C241.
[14] W. Carver, E.C. Goldsmith, Biomed. Res. Int. 2013 (2013).
[15] H. Kuivaniemi, G. Tromp, D.J. Prockop, FASEB J. 5 (1991) 2052.
[16] C.T. Mierke, Prog. Phys. 77 (2014) 076602.
[17] P.A. Janmey, R.T. Miller, J. Cell Sci. 124 (2011) 9.
[18] P.A. Janmey, R.G. Wells, R.K. Assoian, C.A. McCulloch, Differentiation 86 (2013) 112.
[19] P.V. Bayly, R.J. Okamoto, G. Xu, Y. Shi, Phys. Biol. 10 (2013) 016005.
[20] S. Majkut, T. Idema, J. Swift, C. Krieger, A. Liu, D.E. Discher, Curr. Biol. 23 (2013) 2434.
[21] B. Moulia, J. Exp. Bot. 64 (2013) 4617.
[22] A. Peaucelle, S.A. Braybrook, L. Le Guillou, E. Bron, C. Kuhlemeier, H. Hofte, Curr. Biol. 21 (2011) 1720.
[23] S. Rangarajan, L. Madden, N. Bursac, Ann. Biomed. Eng. 42 (2014) 1391.
[24] M. Unbekandt, P.M. del Moral, F.G. Sala, S. Bellusci, D. Warburton, V. Fleury, Mech. Dev. 125 (2008) 314.
[25] S.E. Lindsey, Front. Physiol. 5 (2014) 1.
[26] J. Xi, M. Khalil, N. Shishechian, T. Hannes, K. Pfannkuche, H. Liang, A. Fatima, M. Haustein, F. Suhr, W. Bloch, M. Reppel, T. Sarić, M. Wernig, R. Jänisch, K. Brockmeier, J. Hescheler, F. Pillekamp, FASEB J. 24 (2010) 2739.
[27] B.A. Filas, V.D. Varner, D.A. Voronov, L.A. Taber, J. Vis. Exp. (2011).
[28] L. Davidson, R. Keller, Methods Cell Biol. 83 (2007) 425.
[29] C.S. Roy, J. Physiol. 3 (1881) 125.
[30] F.C. Minozzo, B.M. Baroni, J.A. Correa, M.A. Vaz, D.E. Rassier, Sci. Rep. 3 (2013) 2320.
[31] C. Wiebe, G.W. Brodland, J. Biomech. 38 (2005) 2087.
[32] A.R. Harris, J. Bellis, N. Khalilgharibi, T. Wyatt, B. Baum, A.J. Kabla, G.T. Charras, Nat. Protoc. 8 (2013) 2516.
[33] S.S. Segal, B.R. Duling, Am. J. Physiol. 256 (1989) H838.
[34] https://sites.google.com/site/oliviercardoso/Home/plugins.
[35] L.R.B. Feynman Richard P, L. Sands Matthew, The Feynman Lectures on Physics, Volume II (1969).
[36] R.M. Statics, Nature 435 (2005).
[37] N.R. Chevalier et al., unpublished results.
[38] http://imagingbook.com/.
[39] S.T. JM Gere, Mechanics of Materials, Nelson Thornes Ltd, 1999.
[40] M. Delarue, F. Montel, D. Vignjevic, J. Prost, G. Cappello, M. Curie, I. Curie, Biophys. J. 107 (2014) 1821.
[41] D.A. Narmoneva, J.Y. Wang, L.A. Setton, Biophys. J. 81 (2001) 3066.
[42] R.E. Day, P. Kitchen, D.S. Owen, C. Bland, L. Marshall, A.C. Conner, R.M. Bill, M.T. Conner, Biochim. Biophys. Acta – Gen. Subj. 1840 (2014) 1492.
[43] M.T. Frey, A. Engler, D.E. Discher, J. Lee, Y.L. Wang, Methods Cell Biol. 83 (2007) 47.
[44] D.J. Müller, Y.F. Dufrêne, Trends Cell Biol. 21 (2011) 461.
[45] J.Y. Rho, T.Y. Tsui, G.M. Pharr, J. Biomech. 31 (1998) 21.
[46] M. Stolz, U. Aebi, D. Stoffler, Biol. Med. 3 (2007) 53.
[47] A.J. Engler, L. Richert, J.Y. Wong, C. Picart, D.E. Discher, Surf. Sci. 570 (2004) 142.
[48] T. Reichlin, A. Wild, M. Dürrenberger, A.U. Daniels, U. Aebi, P.R. Hunziker, M. Stolz, J. Struct. Biol. 152 (2005) 52.
[49] C.A. Grant, N.H. Thomson, M.D. Savage, H.W. Woon, D. Greig, J. Mech. Behav. Biomed. Mater. 4 (2011) 535.

[50] Y.M. Efremov, E.A. Pukhlyakova, D.V. Bagrov, K.V. Shaitan, Micron 42 (2011) 840.
[51] J. Henkels, J. Oh, W. Xu, D. Owen, T. Sulchek, E. Zamir, Ann. Biomed. Eng. 41 (2013) 421.
[52] L. Davidson, R. Keller, Elsevier, 2007 (p. 425).
[53] S. Nawaz, P. Sánchez, K. Bodensiek, S. Li, M. Simons, PLoS One 7 (2012).
[54] M.J. Rosenbluth, W.A. Lam, D.A. Fletcher, Biophys. J. 90 (2006) 2994.
[55] E. Spedden, C. Staii, Int. J. Mol. Sci. 14 (2013) 16124.
[56] T.G. Kuznetsova, M.N. Starodubtseva, N.I. Yegorenkov, S.A. Chizhik, R.I. Zhdanov, Micron 38 (2007) 824.
[57] J.L. Hutter, J. Chen, W.K. Wan, S. Uniyal, M. Leabu, B.M.C. Chan, J. Microsc. 219 (2005) 61.
[58] J. Yao, V.D. Varner, L.L. Brilli, J.M. Young, L.A. Taber, R. Perucchio, J. Biomech. Eng. 134 (2012) 024502.
[59] F. Gao, D. Liao, A.M. Drewes, H. Gregersen, Neurogastroenterol. Motil. 21 (2009).